



Supplement of

Characterization of fog microphysics and their relationships with visibility at a mountain site in China

Quan Liu et al.

Correspondence to: Xiaojing Shen (shenxj@cma.gov.cn) and Junying Sun (jysun@cma.gov.cn)

The copyright of individual parts of the supplement might differ from the article licence.

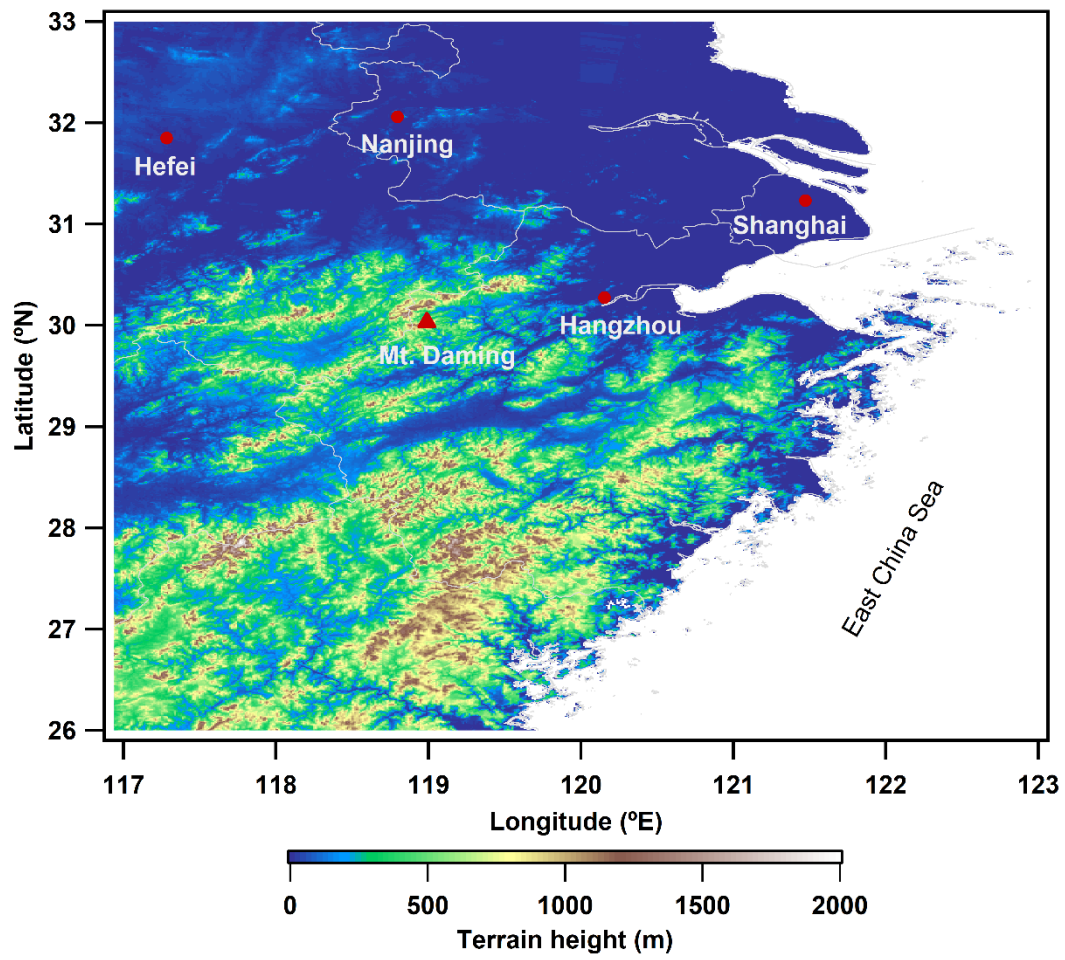


Fig. S1 Location and terrain of the Mt. Daming observation site (triangle symbol).

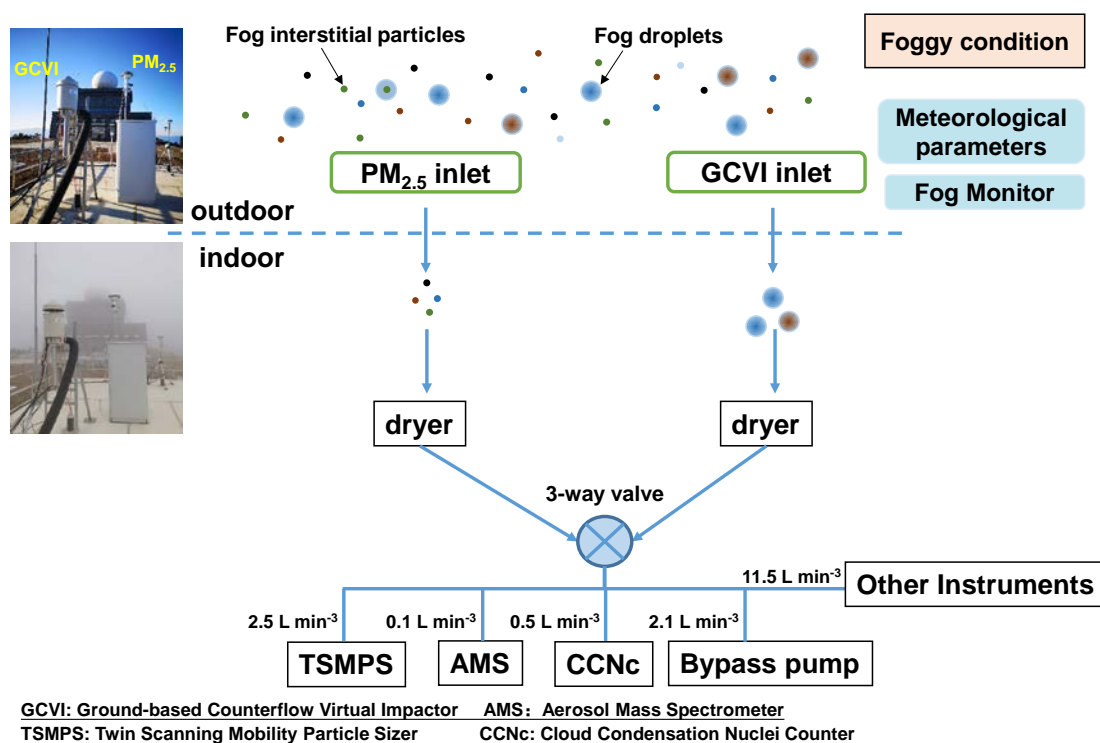


Fig. S2. Schematic of the experimental setup at the Daming Mountain site. An automatic three-way switching system was placed between the sample inlets and instruments. Meteorological parameters and fog droplets were simultaneously measured on the roof of the observation container. The bypass pump only operated when the three-way valve connected to the PM_{2.5} inlet. Its flow rate was controlled at 4.5 L min⁻¹ via a mass flow controller, ensuring the total sample flow reached the 16.7 L min⁻¹ required by the PM_{2.5} cyclone inlet.

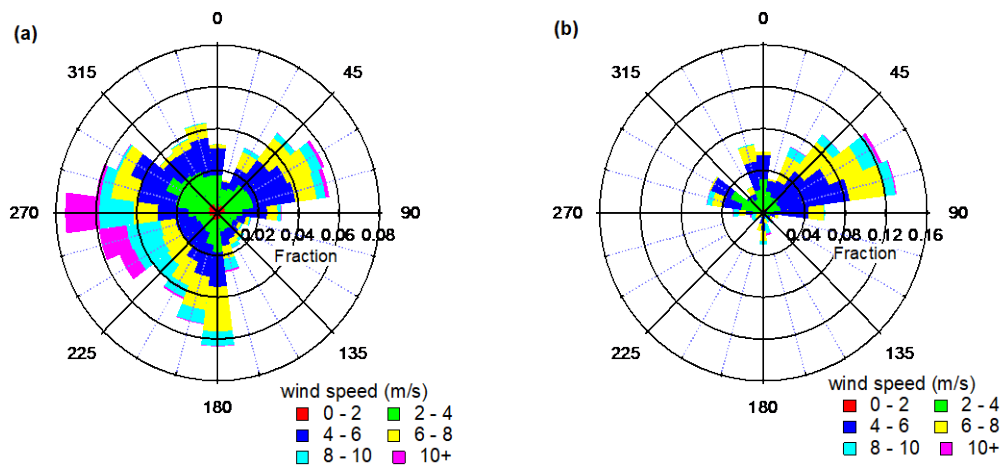


Fig. S3. Wind rose plots during (a) the whole observation period, (b) fog periods.

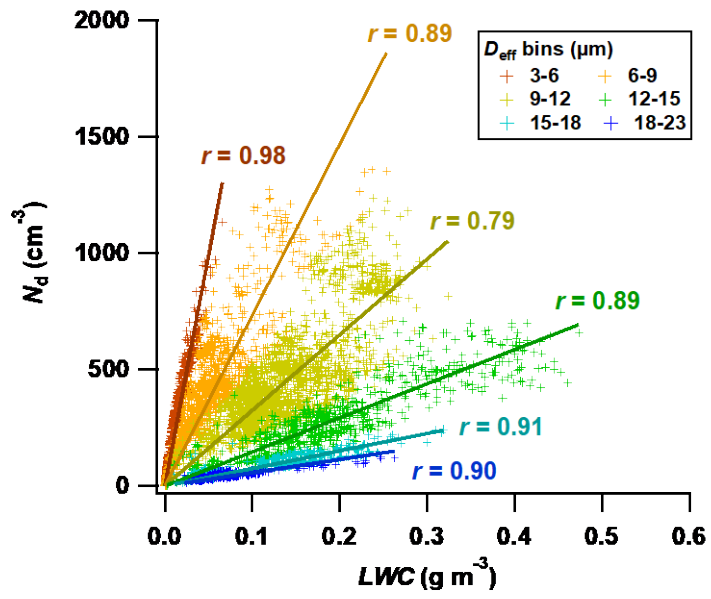


Fig. S4. Relationship between N_d and LWC within different D_{eff} bins.

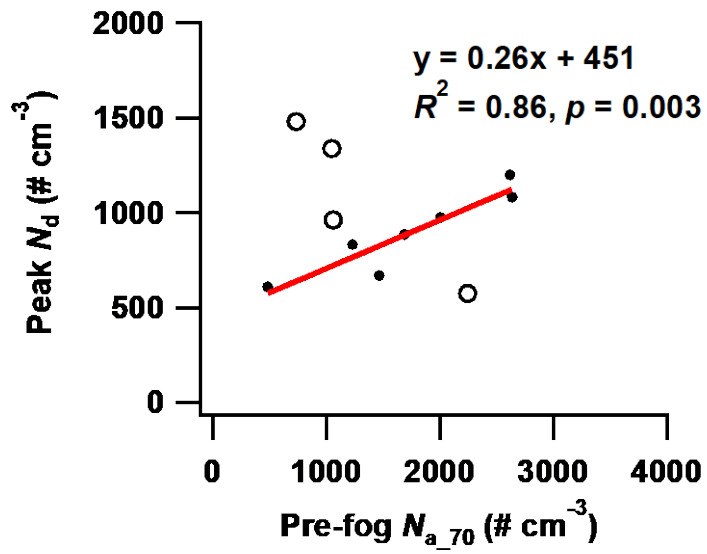


Fig. S5. Peak N_d value for each fog event vs. Pre-fog N_a in the last hour before the event, measured by TSMPS with the size range larger than 70 nm. Hollow circles represent fog events occurring after precipitation, which are excluded from the correlation analysis.

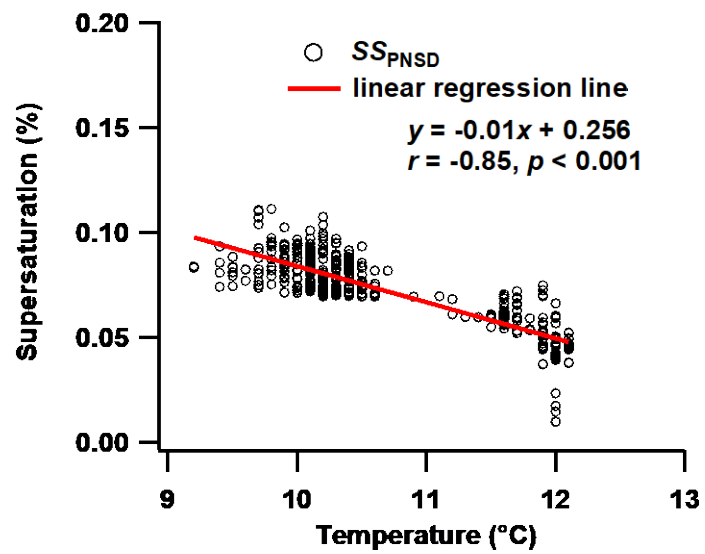


Fig. S6. The relationship between supersaturation (SS_{PNSD}) and temperature for E3.

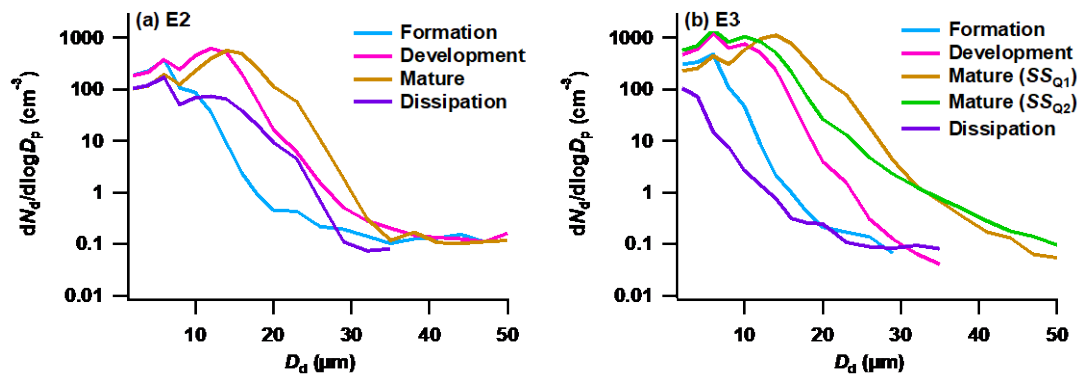


Fig.S7. Evolutions of fog droplets size distribution (DSD) at various stages during (a) E2 and (b) E3, respectively.

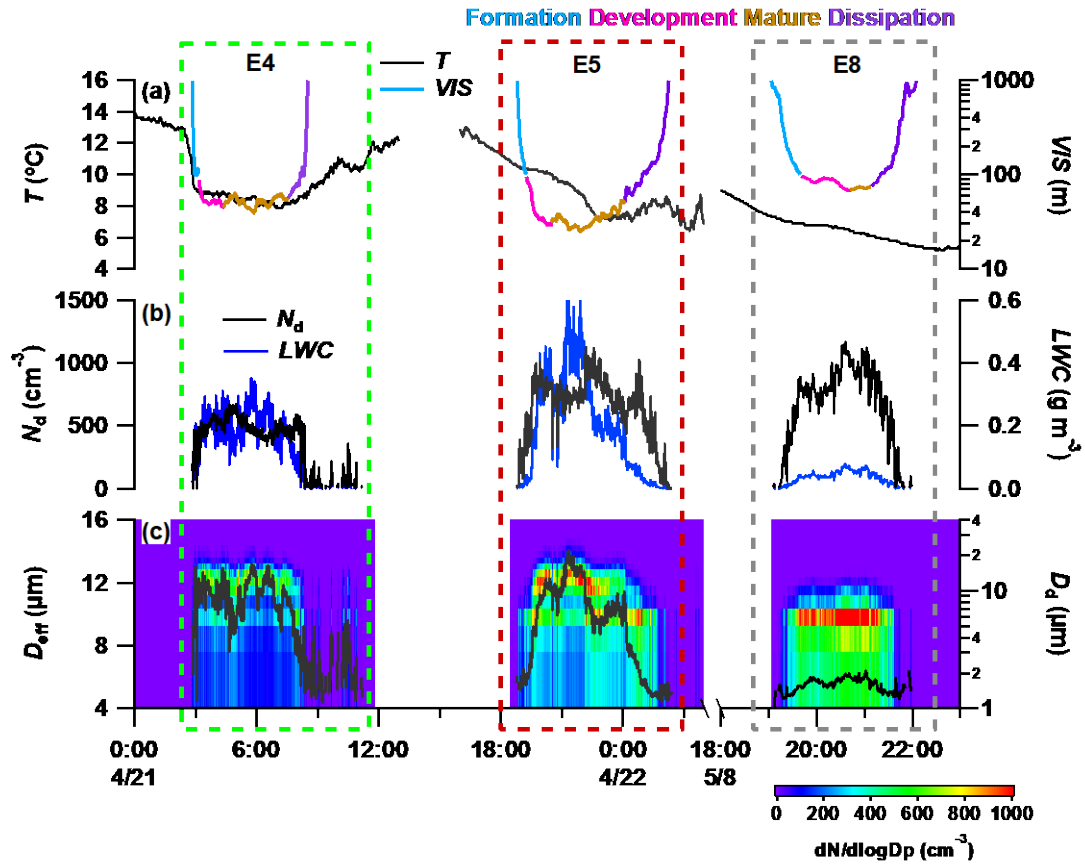


Fig. S8. Temporal evolution of temperature, visibility, fog microphysical parameters, and droplets size distribution for E4, E5, and E8. The colored lines separate each fog event into four stages based on the evolution of visibility.

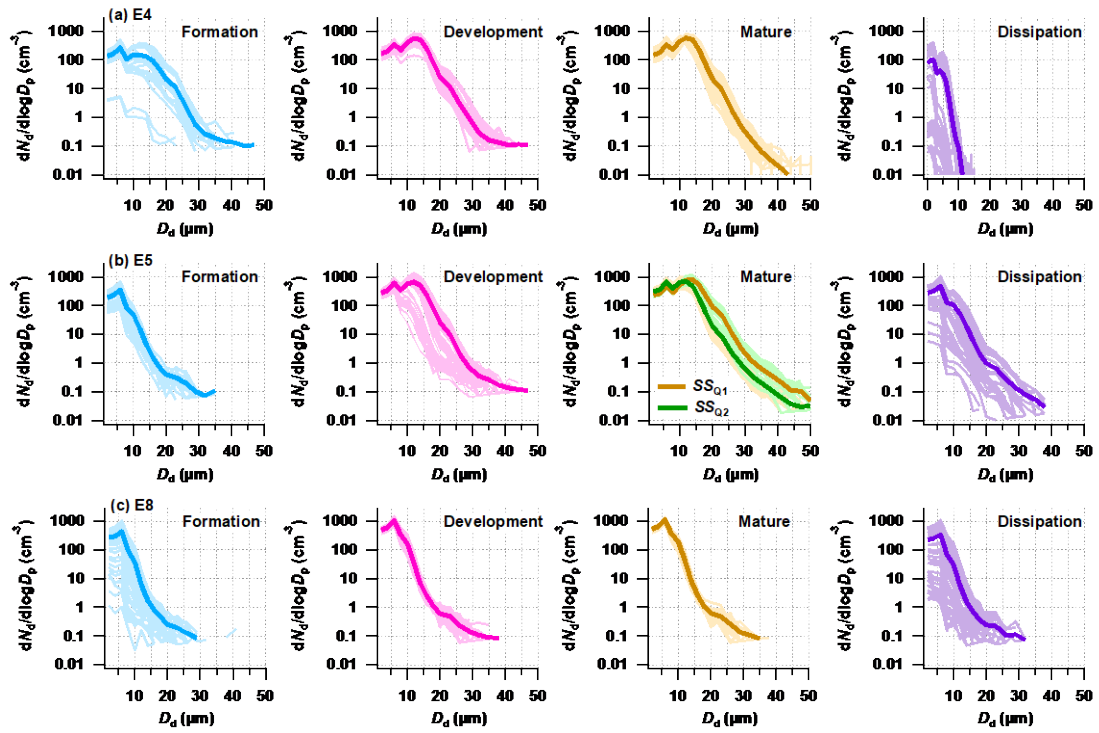


Fig. S9. Evolutions of fog droplets size distribution (DSD) at various stages during (a) E4, (b) E5, and (c) E8, respectively. Thin lines in each stage represent 1-min averaged DSDs, while the thick line is their average.

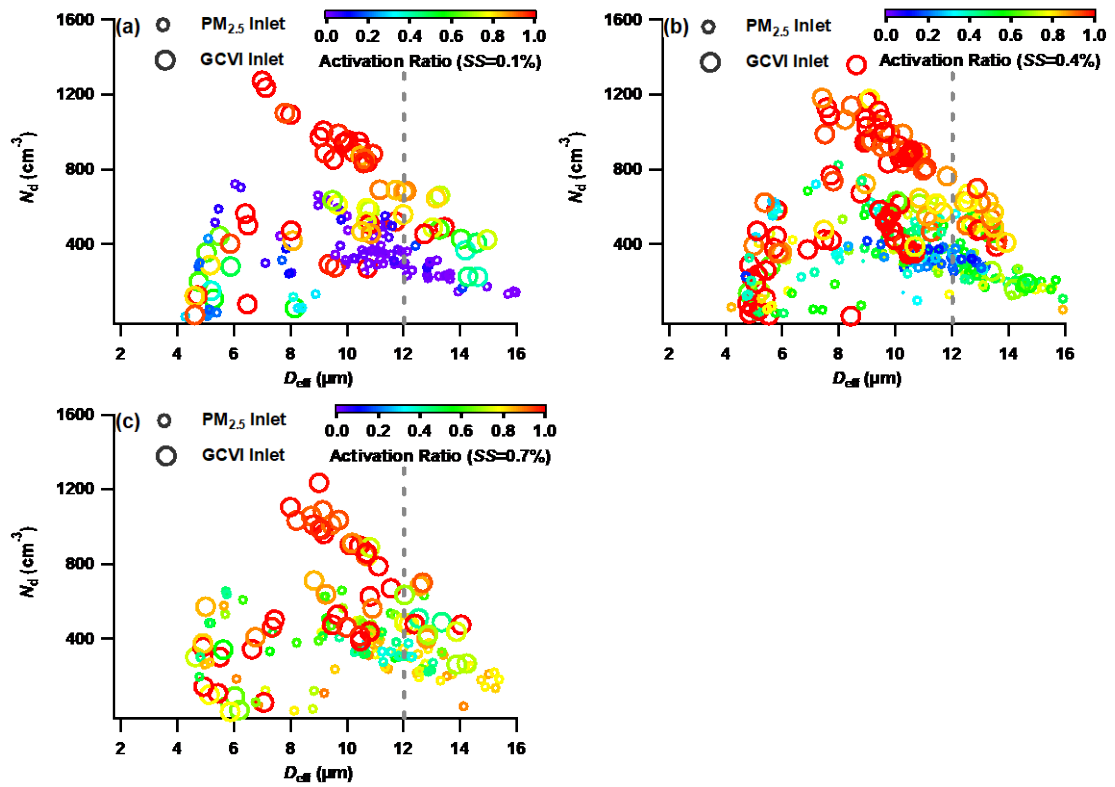


Fig. S10. Differences in CCN activity between fog residual particles (GCVI inlet) and fog interstitial particles (PM_{2.5} inlet), and their variations with fog microphysical parameters: (a) $SS=0.1\%$, (b) $SS=0.4\%$, and (c) $SS=0.7\%$. The gray dash line indicates significant collision-coalescence processes occurring when D_{eff} exceeds 12 μm .

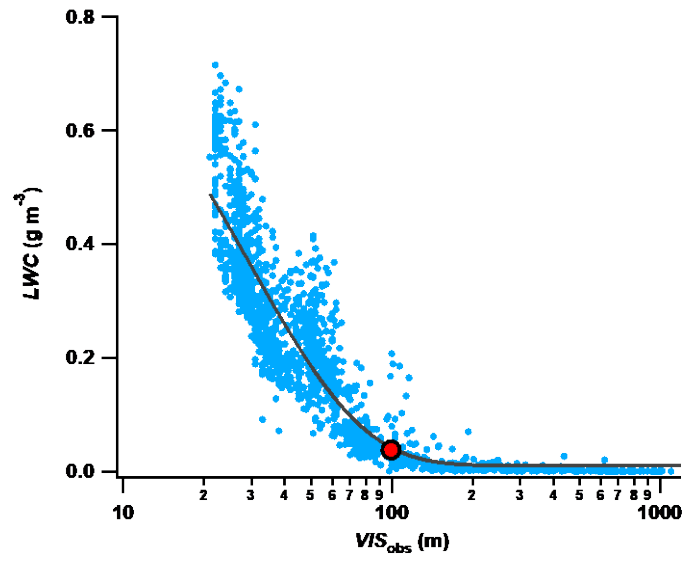


Fig. S11. The relationship between LWC and VIS_{obs} during this campaign. The red circle indicates the inflection point in the power-law fitting curve.

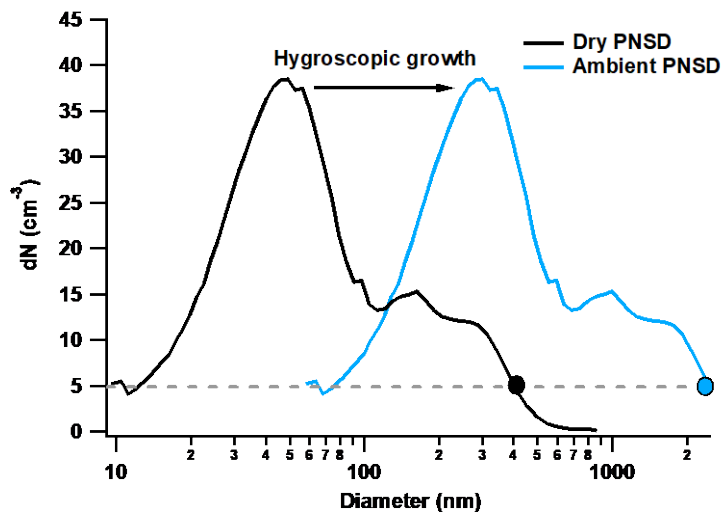


Fig. S12. Schematic of estimating bulk hygroscopic growth factor (GF) of fog interstitial particles. The black circle represents the maximum dry diameter measured in fog interstitial particles, with a corresponding number concentration of not less than 5 cm^{-3} . The blue circle represents the cut-size of $\text{PM}_{2.5}$ cyclone inlet, which defined as the maximum diameter of ambient PNSD after hygroscopic growth. Upon this, the bulk GF in this case approximates to 6.1.

Table S1. Density, hygroscopicity parameter (κ) and refractive indices of pure composition used in this study.

Species	Density (kg m ⁻³)	κ	Refractive index
NH ₄ NO ₃	1725	0.68	1.6 – 0 <i>i</i>
(NH ₄) ₂ SO ₄	1769	0.52	1.53 – 0 <i>i</i>
NH ₄ HSO ₄	1780	0.56	1.47 – 0 <i>i</i>
Organics	1400	0.1	1.46 – 0.021 <i>i</i>
Black Carbon	1800	0	1.85 – 0.79 <i>i</i>
Water	1000		1.3+0 <i>i</i>